IMPROVED LONG TERM CYCLING OF POLYAZULENE/REDUCED GRAPHENE OXIDE COMPOSITES FABRICATED IN A CHOLINE BASED IONIC LIQUID

Milla Suominen[a,*], Pia Damlin[a,*], Sari Granroth[b], Carita Kvarnström[a]

[a] Turku University Centre for Materials and Surfaces (MATSURF), Laboratory of Materials Chemistry and Chemical Analysis, University of Turku, FIN-20014 Turku, Finland

[b] Laboratory of Materials Science, University of Turku, FIN-20014 Turku, Finland

Abstract

To improve the energy density of supercapacitors, novel electronically conducting polymers should be introduced to the research field. Polyazulene is a well-suitable candidate as it exhibits good capacitive behavior both in organic solvents as well as in various ionic liquids, but especially its long term cycling stability should be improved. Previously, enhanced properties have been obtained by combining conducting polymers with carbon nanomaterials to fabricate composites. This work presents an ionic liquid assisted electrochemical polymerization and characterization of polyazulene-reduced graphene oxide composites. The ionic liquid of our choice is choline-based liquid salt. We prepared stable dispersions of graphene oxide in this ionic liquid and performed potentiodynamic electropolymerization of azulene in the mixture. Changing the concentration of graphene oxide between 0.1 and 2 mg mL^{-1} had no remarkable effect on the polymerization or electrochemical behavior of the composite materials. The composites exhibit higher capacitances compared to neat polymer films determined by cyclic voltammetry and electrochemical impedance spectroscopy. The obtained films also exhibit excellent cycling stabilities retaining over 90 % of their initial capacitance with tendency towards improved cycling stability when combined with reduced graphene oxide. The successful incorporation and reduction of graphene oxide was determined by several spectroscopic techniques.

1. Introduction

In past years, composites have become important in obtaining light weight but exceedingly strong materials for aircrafts, vehicles and sports equipment, but they can also offer advantages in organic electronics components. Electronically conducting polymers (ECPs) are favored in various electronics applications, including energy storage devices, because of their accessibility, low price and flexibility, but due to swelling and shrinking occurring upon their charging/discharging, ECPs

* Corresponding author. Tel: +358 50 437 0081. E-mail: milsuo@utu.fi (Milla Suominen)
* Corresponding author. Tel: +358 50 328 5468. E-mail: pia.damlin@utu.fi (Pia Damlin)

can lose their properties rather quickly [1]. Incorporating carbon nanotubes (CNTs) into ECPs has been shown to enhance the mechanical stability but also improve the electronic properties [2,3], but since CNTs are an expensive choice for commercial applications, the ideas have been implemented into cheaper carbon nanomaterials, i.e. graphene. Graphene possesses uniquely high reactive surface area, good conductivity, and excellent thermal, mechanical and chemical stability [4,5] and, when produced by consecutively oxidizing and reducing graphite into chemically modified graphene sheets, it can also be produced in large quantities at low price [6].

Supercapacitors compete with conventional batteries in the market with their superior life times and power capabilities [7], but pure graphene or ECP based devices lack the high energy content or the long cycle life, respectively. In supercapacitor application, composites of different carbon nanomaterials and ECPs have shown promise [8]. A composite of polyaniline (PANi) and chemically reduced graphene oxide (rGO) showed a high specific capacitance of 480 F g^{-1} compared to the value of 420 F g^{-1} for the neat polymer film under the same conditions [9]. After five cycles, the capacitance of neat polymer film had dropped to 280 F g^{-1} while composite still retained 410 F g^{-1}, and after 1000 cycles the composite still showed 70 % of its initial capacitance. Specific capacitances of 108, 249 and 361 F g^{-1} were reported for rGO composites with poly(3,4-ethylenedioxythiophene) (PEDOT), polypyrrole (PPy) and PANi, respectively [10]. After 1000 charging/discharging cycles, all of the abovementioned composites retained over 80 % of their initial capacitance whereas PANi fibers' capacitance decreased to 68 % after only 600 cycles. Electrochromic applications have also been reported to gain lifetime improvements upon combination with rGO [11].

Generally, the composites are fabricated by a chemical route: the polymer is polymerized by chemical oxidative polymerization and graphene oxide (GO) is reduced by strong reducing agents [8]. Chemical fabrication techniques may have the advantage of simple scalability, but electrochemical techniques offer a versatile way to control the structure of the final product and an eco-friendlier technique by which the composite materials can be directly coated on conducting substrates without additional steps [12,13]. Since the solvent, the electrolyte salt and any additives in the electrolyte solution have huge effect on the film microstructure and thus its electrochemical activity, a variety of materials can be obtained by electrochemical techniques [14–16]. The use of ionic liquids (ILs), for example, results in denser microstructure which boosts the electroactivity [17]. Since GO sheets are decorated with various negatively charged oxygen functional groups, it can be incorporated in the polymer film as a counter anion during electropolymerization [12,18–20]. Additionally, weak π-π as well as electrostatic interactions between the negatively charged GO and positively charged radical cations as well as purely physical entrapment are possible [19]. GO

can then be efficiently reduced inside the film via electrochemistry thus avoiding the use of toxic reducing agents [12,21]. Previously, composites of ECPs and electrochemically reduced graphene oxide (ErGO) have been successfully fabricated in aqueous [11,19,21] and ionic liquid media [12].

Azulene is an intriguing aromatic, non-benzenoid hydrocarbon which is studied for non-linear optics, solar cells and dyads due to its unique charge transfer properties [22,23]. Azulene can be polymerized chemically [24] and electrochemically [17,25–29] to polyazulene (PAz) depicted in Scheme 1a, and has been used in all-solid-state ion selective electrodes [30] and supercapacitors [27,29] because it possesses high intrinsic pseudocapacitance. Although PAz already exhibits high capacitance, its cycling stability requires improvement [26]. By using ILs during polymerization and doping, an improvement in cycling stability compared to films produced and cycled in organic solvents has been recently reported [27,29]. PAz has been previously combined by electrochemical techniques with TiO_2 [25,26], fullerene [17] and polybenzimidazobenzophenanthroline-poly(ethyleneoxide) (BBL-PEO) [28] for improved electron transfer in organic solar cells.

In this work, composite materials of polyazulene and electrochemically reduced graphene oxide were fabricated in a choline based ionic liquid using a facile electrochemical polymerization technique to obtain high energy material with improved long term cycling stability. The IL [Choline][TFSI] (Scheme 1b), also known as $[N_{1112(OH)}][Ntf_2]$ and N,N,N-trimethyl-N-(2-hydroxyethyl)ammonium bis(trifluoromethanesulfonyl)imide, chosen for this work has been previously studied for example in polymer electrolytes and actuators due to the good electrochemical stability of the anion and the biocompatible nature of the cation [31,32]. The electrochemical performance, with emphasis on the capacitive behavior, was determined in three-electrode configuration using cyclic voltammetry (CV) and electrochemical impedance spectroscopy (EIS). The structure of different materials was determined by infrared spectroscopy (IR), Raman spectroscopy, X-ray photoelectron spectroscopy (XPS) and scanning electron microscopy (SEM) techniques. The results show clearly improved capacitance as well as improved cycling stability over neat polymer material.

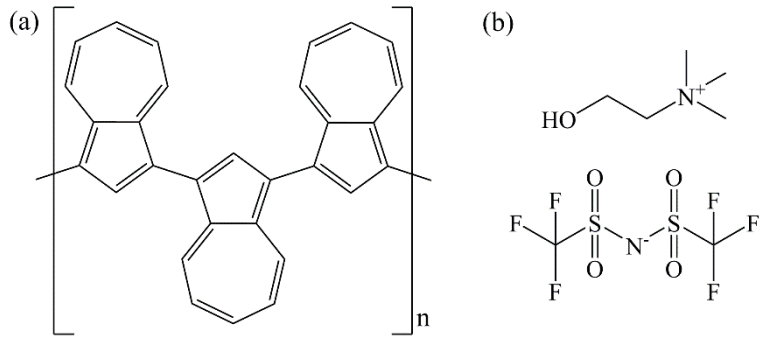

Scheme 1. The chemical structures of (a) PAz and (b) [Choline][TFSI].

2. Experimental

2.1 Materials

Ferrocene (Aldrich, 98 %), azulene (Aldrich, 99 %) and choline bis(trifluoromethylsulfonyl)imide [Choline][TFSI] (Iolitech, 99 %) were all used without further purification steps. [Choline][TFSI] was stored in argon filled glove box and dried in vacuum oven (45 °C, ≥ 2 h) prior to use, while ferrocene and azulene were stored under ambient conditions. Water content of [Choline][TFSI] was determined by Karl Fisher titration and the results are presented in Fig. S3, and the conductivity reported by the manufacturer is 3.978 mS cm^{-1} at 45 °C.

2.2 Preparation of GO dispersions in ionic liquids

GO was synthesized from natural graphite flakes (Alfa Aesar, mesh 325, 99.8%) using a modified Hummer's method [6]. Our GO synthesis procedure as well as the procedure for the preparation of GO/IL –mixtures has been elaborated before [12]. A short description of the GO/[Choline][TFSI] dispersions as well as representative analysis results are presented in the supplementary information.

2.3 Electrode preparation

All electrochemical measurements were conducted using a conventional three-electrode configuration where a silver wire coated with AgCl served as quasi reference electrode (calibrated vs. Fc^0/Fc^+, E_{REF} = 0.12 V) and a coiled Pt wire as the counter electrode in all experiments. Pt-minielectrode, tin oxide glass (SnO_2) and Si wafers were applied as working electrodes. A Pt-minielectrode was polished mechanically with diamond pastes from 3 to 0.25 µm (Struers A/s) and rinsed with quartz distilled water and ethanol. SnO_2 glass substrates with sheet resistance of 8.1 Ω cm^2 (Pilkington) were cleaned by ultrasonication in acetone, ethanol and quartz distilled water successively for 10 min. Si wafers (Okmetic) were cleaned in hot piranha solution (1:3 30% H_2O_2 and conc. H_2SO_4) overnight, rinsed with quartz distilled water and dried before an approximately 100 nm layer of gold was evaporated on top of the wafers (Edwards coating system). The gold coated wafers were further cleaned with argon plasma prior to use.

2.4 Electropolymerization and electrochemical characterization

Films were deposited using cyclic voltammetry where the potential was cycled between -0.7 and 1.1 V at 50 mV s^{-1} scan rate until a charge density of approximately 445 mC cm^{-2} was reached. Azulene

concentration was kept constant (50 mM) while GO concentration was varied between 0.1 and 2 mg mL^{-1}. Before electrodeposition, the GO/IL dispersions and neat IL were dried in vacuum oven at 45 ºC for 2 h. All electrolytes were deaerated with dry N_2 before and during electrochemical experiments.

After polymerization, the deposited films were rinsed with and emerged into monomer-free IL. The electrochemical behavior was studied using cyclic voltammetry for films after polymerization, electroreduction and long term cycling using two potential ranges (-0.6 - 0.8 V and 0.0 - 0.8 V) and several scan rates (20, 50, 100, 150 and 200 mV s^{-1}). GO was electrochemically reduced by cycling the composite films between -0.5 and -1.9 V over 10 cycles at 50 mV s^{-1} scan rate. In all CV experiments, Autolab PGSTAT101 potentiostat with Nova 1.11 software was used and the experiments were performed at +32 ºC due to problems with solidification of [Choline][TFSI] near room temperature (18-20 ºC). The melting point of [Choline][TFSI] has been reported to be 21 °C [31]. Impedance spectra were acquired using IviumStat potentiostat in the frequency range from 100 kHz to 100 mHz using 97 frequencies and 10 mV amplitude.

2.5 Structural characterization

For IR, Raman and SEM analysis, the films were polymerized on SnO_2 glass substrates. The films were thoroughly rinsed with dichloromethane and ethanol to remove excess ionic liquid before structural characterization. The IR spectrum of GO was obtained by drying a drop of 1 mg mL^{-1} GO aqueous solution on a SnO_2 glass. IR spectra were recorded with a Bruker Vertex 70 FTIR spectrometer equipped with liquid nitrogen cooled MCT detector. The spectra were measured at an incidence angle of 55^o relative to the surface normal using a Harrick Seagull variable angle reflection accessory. For each spectrum, 124 scans at 4 cm^{-1} spectral resolution were recorded. SEM images were recorded using LEO (Zeiss) Gemini 1530 FEG-SEM. Raman spectra were measured by Renishaw inVia QONTOR Raman microscope equipped with Leica microscope and a CCD detector using excitation wavelengths of 785 and 532 nm, 20x objective and 1200 l/mm grating. For elemental analysis, the films were deposited on gold coated Si-wafers, and the XPS spectra were obtained by Perkin-Elmer PHI 5400 spectrometer using Mg Kα excitation (1253.6 eV). The binding energy scale was calibrated by setting the binding energy of the Au $4f_{7/2}$ photoemission line of the calibration sample to 84.0 eV. The XPS spectra were fitted using Shirley background removal and Voigt line shape.

3. Results and discussion

3.1 Electrochemical preparation of PAz/ErGO composite films

Fig. 1 shows representative multicycle voltammograms obtained during potentiodynamic deposition of PAz/GO composite films in [Choline][TFSI], where GO concentration is varied between 1 (Fig. 1a) and 2 mg mL^{-1} (Fig. 1b). Changing the GO concentration has no significant effect on the monomer oxidation or film deposition rate. All voltammograms exhibit trace-crossing in the first anodic sweep and a continuous current increase during polymerization. In the consecutive cycles, mainly two oxidation responses are detected in the anodic potential sweeps (0.0 and 0.55 V) and one reduction response during the cathodic sweeps (-0.05 V). After approximately 10 to 15 polymerization cycles, the peak-to-peak separation ΔE ($\Delta E = E_{ox} - E_{red}$) is increasing, which is attributed to slower redox processes as the films become thicker.

To partially restore the aromatic structure and recover the conductive properties of graphene, the composite films were electrochemically reduced by cyclic voltammetry. In our previous work, the number of reduction cycles was set to 30 to ensure efficient reduction of GO, but already after 10 reduction cycles we observed almost maximal increase in capacitive performance of the reduced composite film [12]. Additionally, in earlier works a potentiostatic reduction at -0.85 V for 10 minutes has been deemed sufficient [21]. To study the reduction of GO in [Choline][TFSI], a drop of diluted GO aqueous solution (c_{GO} = 1 mg mL^{-1}) was dried on SnO_2 glass and 10 potential scans in the range 0.0 - (-1.9) V at 50 mV s^{-1} scan rate was applied. The resulting voltammogram is presented in Fig. S4a and shows a broad capacitive signal in the first cathodic sweep beginning at -0.5 V. In consecutive cycles, no distinctive features are observed and the current response is reduced. After electroreduction, a color change from a light brown to dark brown was detected which is consistent with GO reducing to a graphene-like material. Since PAz might undergo irreversible structural changes during prolonged cycling to very negative potentials [26], the number of reduction cycles in this particular study was limited to 10. Fig. S4b illustrates the five first electroreduction CVs of PAz and PAz/GO composite films. In the first cycle, a capacitive current response is obtained and consecutive cycles are rather featureless both for PAz and its composite with GO. The capacitive current is, however, higher for the composite than for the polymer which could be an indication of GO. Broad signals exhibited in both CVs during the first cathodic sweep (for PAz at -0.8 V and for composite at -0.7 V) are related to the polymer [33].

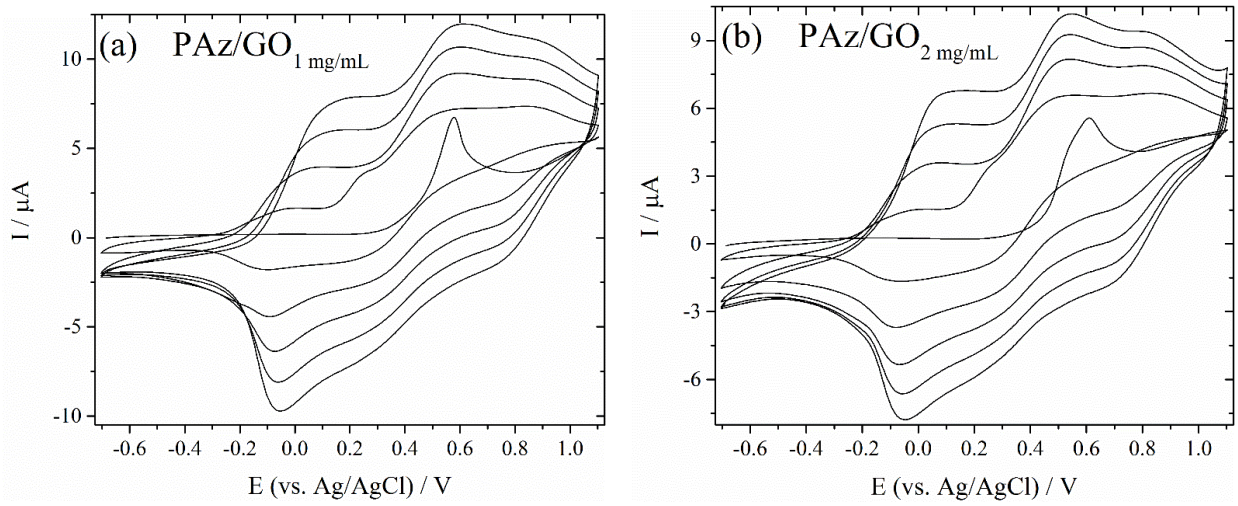

Fig. 1 Multicycle voltammograms of PAz/GO composite synthesis at Pt electrodes using 1 mg mL^{-1} (a) and 2 mg mL^{-1} (b) concentrations of GO in [Choline][TFSI]. Potential was scanned between -0.7 and 1.1 V (vs. Ag/AgCl) at 50 mV s^{-1} scan rate until a charge density of approximately 445 mC cm^{-2} was reached. First five cycles are presented.

3.2 Characterization of the composite materials

3.2.1 Morphology

SEM images of neat PAz film as well as PAz/GO and PAz/ErGO composite films are presented in Fig. 2. The morphology of PAz is even and granule-like (Fig. 2a) while the SEM images of PAz/GO (Fig. 2b) and PAz/ErGO (Fig. 2c-d) materials reveal large sheets of GO in the structure. In addition, changes in the microstructure of the composites before and after electroreduction are clear. PAz/GO composite shows a layer of crumpled sheets distributed over the entire analyzed area which resembles other ECP/GO composites fabricated electrochemically in aqueous solutions [12,18,20,21]. Interestingly, the morphology of the composite changes drastically after reduction; PAz/ErGO film shows sheets of reduced GO scattered evenly in the granule-like polymer network. Some of the polymer has clearly deposited on top of the ErGO sheets (Fig. 2d) which indicates that GO sheets have been successfully incorporated inside the film, as well. When ECP/GO composites are electropolymerized from aqueous solutions, GO usually acts solemnly as the doping anion and is thus incorporated effectively in the film, but upon using ILs as electrolyte solution, anions of the IL are expected to act as primary doping anions and GO sheets incorporate into the film by mechanical entrapment and due to weak π-π and/or cation-π interactions. Therefore, the sheets observed in Fig. 2b could be only weakly bound to the surface and the interactions could be further altered during the electroreduction. To obtain good resolution SEM images, the films underwent an

exhausting washing procedure to remove all excess IL from the films, and any loosely bound sheets might have rinsed away during the washing.

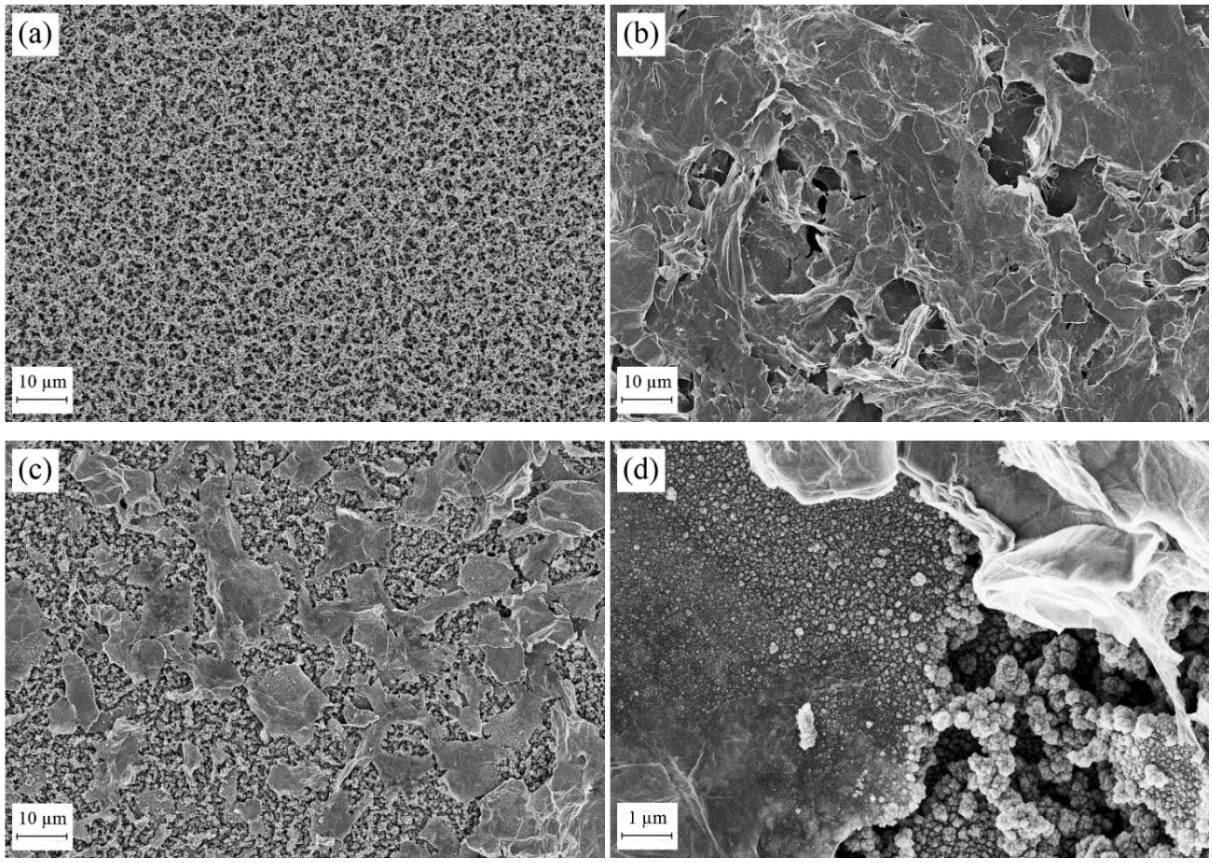

Fig. 2 SEM images of (a) PAz film, (b) PAz/GO and (c-d) PAz/ErGO composite films. Magnifications: 1000x (a-c) and 10000x (d).

3.2.2 Electrochemical behavior of PAz/ErGO materials

The p-doping behavior was recorded directly after polymerization and electroreduction to determine the effects of GO addition and reduction on film behavior. In the light of previous results [12,19], it was expected that after polymerization the films would exhibit lower electrochemical activity than PAz films due to poorly conducting GO embedded in the polymer matrix and only after reduction to better conducting ErGO, an increase in the electroactivity of the composite film would be observed. The resulting p-dope CVs are shown in Fig. 3 and 4. As is clearly indicated in Fig. 3, the electroactivity of composite materials is better than for the neat PAz already after polymerization: the redox charges (q_{redox}) are 0.77 mC for PAz, 1.35 mC for PAz/$GO_{0.1\ mg/mL}$ composite and 1.77 mC for PAz/$GO_{1\ mg/mL}$ composite after polymerization (Fig. 3a). Higher electroactivity could be a result of enlarged surface area [19] since large sheets of GO have been implemented in the material

as could be seen from the SEM analysis. After electroreduction, the activity of the composite materials increased (q_{redox} for PAz/ErGO$_{1\ mg/mL}$ 1.84 mC, Fig. 3a) or decreased slightly: q_{redox} 0.90 and 0.82 mC for PAz/GO$_{2\ mg/mL}$ composite before and after reduction, respectively (Fig. 3b), and q_{redox} 1.27 mC for PAz/GO$_{0.1\ mg/mL}$ composite after reduction (Fig. 3a). The decrease in electroactivity is not, however, as profound as observed for PAz. Previously, a decrease in capacitance has been reported for PEDOT [21] and poly(N-methylaniline) [20] composites with rGO in aqueous solution. Slight loss of composite electroactivity is attributed to polymer degradation [26] and changes in morphology.

The onset of polymer oxidation lies at similar potentials for each material but the difference between peak oxidation (E_{pa}) and reduction potentials (E_{pc}), however, is notably larger for composite films: ΔE is 0.2 V for PAz and 0.6 V for PAz/GO$_{1\ mg/mL}$ composite (Fig. 3a). This can be an evidence of the resistive property of GO or the result of thicker films due to GO incorporation. Increased hysteresis could also be related to the microstructure of the materials: compact layer of crumpled GO sheets on top of the unreduced composite could slow down ion diffusion into the film. The dependence of maximum peak currents on the square root of scan rate is linear (Fig. S5) indicating diffusion limited reaction in the composite material. After electroreduction, E_{pa} and E_{pc} of PAz shift to more cathodic potentials while the p-doping response of composite materials remains almost unchanged.

Fig. 4 depicts the p-doping behavior of the composites in the potential range from 0.0 to 0.8 V. When using slow scan rates ($\leq$ 50 mV s^{-1}), the shape of the CVs is ideally pseudo-rectangular, but upon increasing the scan rate the shape clearly deviates from ideal behavior for supercapacitors which is related to high viscosity (93.4 cP at 30 °C [34]) of [Choline][TFSI].

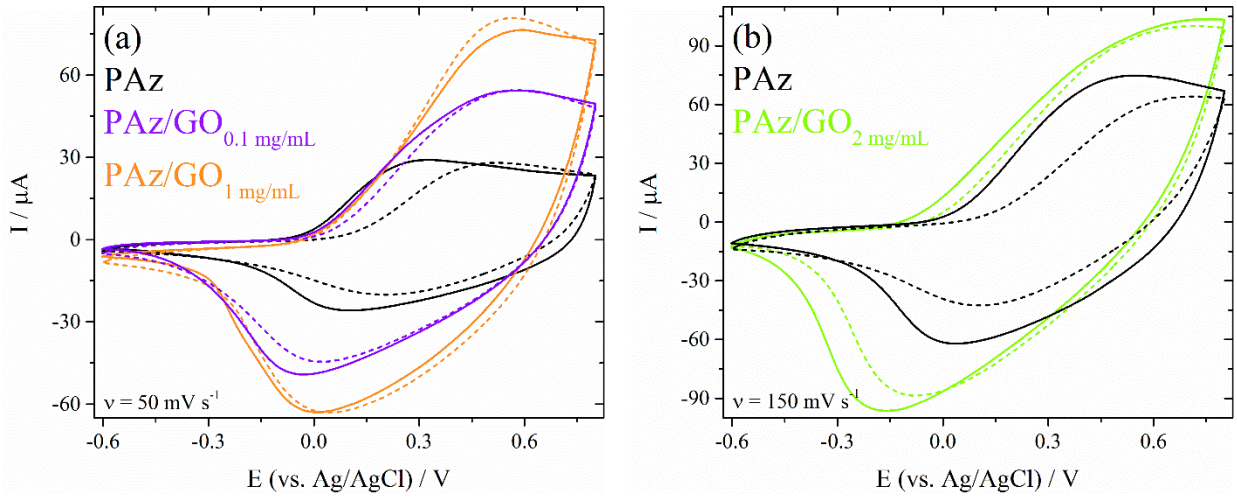

Fig. 3 CVs of p-doping PAz and composite films polymerized using different GO concentrations over polymerization. Scan rate in (a) 50 mV s^{-1} and in (b) 150 mV s^{-1}. The films were cycled between -0.6 and 0.8 V after polymerization (solid lines) and electroreduction (dashed lines).

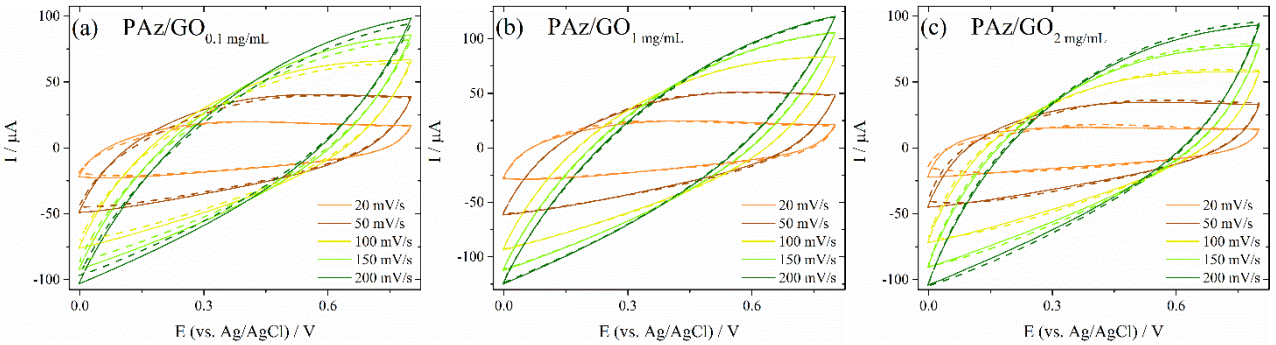

Fig. 4 CVs of p-doping the composites in the potential range 0.0 - 0.8 V with several scan rates. GO concentration over polymerization was (a) 0.1 mg mL^{-1}, (b) 1 mg mL^{-1} and (c) 2 mg mL^{-1}.

Capacitance values were evaluated by integration of the charging half cycle of the CVs in a three-electrode configuration, and the results are presented in Fig. 5. All composites clearly exhibit higher capacitances over neat PAz. As indicated in Fig. 5a and b, where the capacitance has been plotted against several scan rates, all films retained only half of the initial capacitance value at 200 mV s^{-1}. This can be mostly attributed to the high viscosity and consequent low conductivity of the electrolyte [35]. After electroreduction, the composite films did not show changes in their capacitance whereas a slight decrease in the capacitance of PAz is observed. After electroreduction, PAz films showed an average capacitance of 55 ± 7 mF cm^{-2} while composites exhibited capacitances of 94 ± 0.2 mF cm^{-2} ($PAz/GO_{0.1\ mg/mL}$), 130 ± 8 mF cm^{-2} ($PAz/GO_{1\ mg/mL}$) and 93 ± 11 mF cm^{-2} ($PAz/GO_{2\ mg/mL}$) at 20 mV s^{-1} scan rate.

The capacitance retention of different materials during long term cycling is elaborated in Fig. 5c. All materials possess good electrochemical cycling stability over 1200 p-doping cycles retaining over 85 % of their electrochemical activity. A modest tendency towards improved cycling stability for the composite materials can be concluded based on these results, however, the differences between composite materials and the polymer are small. From Fig. 5b, the average capacitances after long term cycling were 50 ± 9 mF cm^{-2} and 123 ± 6 mF cm^{-2} for PAz and $PAz/ErGO_{1\ mg/mL}$ films, respectively.

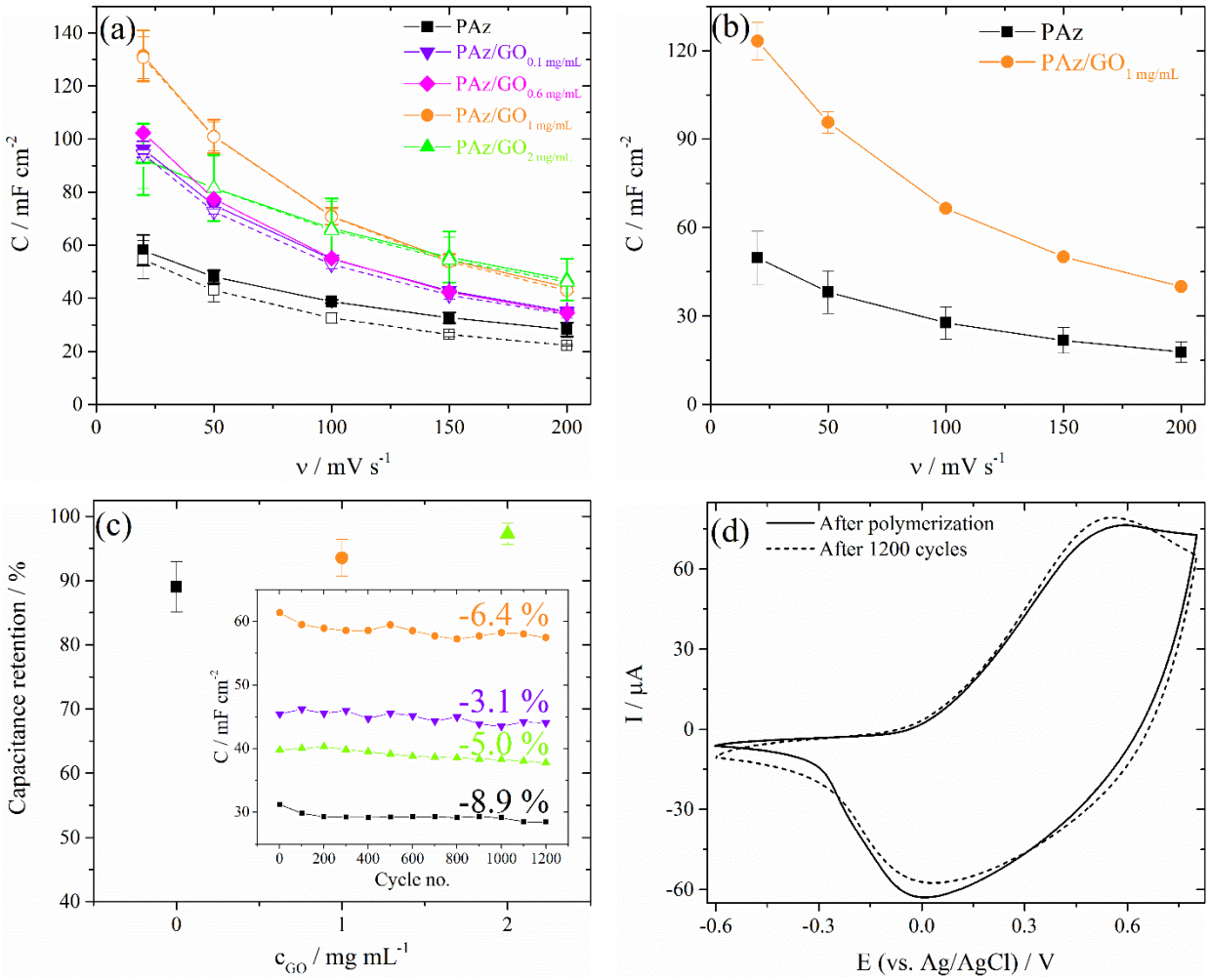

Fig. 5 (a) Dependence of capacitance on scan rate after polymerization (solid line) and electroreduction (dashed line). (b) Dependence of capacitance on scan rate after long term cycling. (c) Capacitance retention over 1200 p-doping cycles in the range 0.0 - 0.8 V at 100 mV s^{-1} scan rate. (d) CVs of p-doping PAz/ErGO$_{1\ mg/mL}$ composite at 50 mV s^{-1} scan rate before (solid line) and after (dashed line) long term cycling.

The complex Nyquist impedance plots recorded at 0.6 V for composite film and PAz are presented in Fig. 6. The Nyquist plots of the films obtained directly after polymerization are alike (Fig. 6a). After electroreduction and long term cycling (Fig. 6b-c), the Nyquist plots of PAz exhibit clear increase in charge transfer resistance related semi-circle in the high and medium frequencies whereas the composite films retain their impeding properties well. In the low frequency capacitive region, however, any significant changes are not detected between GO and ErGO composite materials and neat polymer film. We have previously reported the impeding behavior of PAz before and after long term cycling [29] and related the changes of charge transfer resistance to decrease in electroactivity which is evident from p-doping CVs. The CVs of p-doping PAz/ErGO$_{1\ mg/mL}$

composite before and after electroreduction (Fig. 3a) as well as before and after long term cycling (Fig. 5d) show no remarkable changes in electroactivity of the film, and are thus in good accordance with the results obtained by EIS.

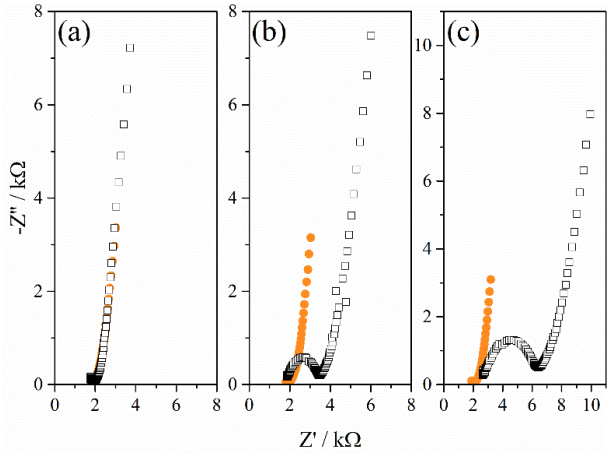

Fig. 6 Complex impedance plots of PAz/ErGO$_{1\ mg/mL}$ composite film (●) and PAz film (□) at 0.6 V directly after polymerization (a), electroreduction (b) and long term cycling (c).

3.2.3 IR spectroscopy

The *ex situ* FTIR spectra of PAz, PAz/GO and PAz/ErGO composite films as well as GO are presented in Fig. 7. All band frequencies with tentative assignments are listed in supplementary information (Table S1). PAz IR spectra (Fig. 7c) exhibits peaks at wavenumbers 1 566, 1 475, 1 392, 1 350 and 1 330 cm^{-1} which are attributed to the stretching of C=C bonds in the aromatic ring. The bands in the range from 1 294 to 1 016 cm^{-1} are attributed to =C-H in-plane deformation vibrations, with the exception of the peak at 1 136 cm^{-1} which probably arises from the doping anion [TFSI], and bands at 1 714, 945, 877 and 740 cm^{-1} are attributed to =C-H out-of-plane deformation vibrations. [25,26] The remaining peaks at 1 454 and 786 cm^{-1} are ascribed to the [Choline] cation [36] and [TFSI] anion [37], respectively. PAz related bands are observed in both composite films' spectra, although the intensity of these peaks is considerably weakened in the PAz/GO composite spectrum (Fig. 7a and b, respectively). This can be explained by the changes observed in microstructure: the surface of PAz/GO composite is completely covered with crumpled sheets of GO with no evidence of polymer present while in the SEM image of the reduced composite a polymer film with granule-like structure is visible alongside evenly embedded ErGO sheets. Additionally, a peak at 1 093 cm^{-1} is observed before and after reduction of the composite and is attributed to the stretching vibrations of C-C and C-O of GO and ErGO. In PAz/GO IR

spectrum, PAz related bands at 1 242 and 1 220 cm^{-1} are not visible which could be due to asymmetric C-O-C stretching vibrations of the epoxide groups of GO at 1 232 cm^{-1}.

GO gives rise to the following well-established bands: a broad band above 3 000 cm^{-1} which is attributed to the stretching vibrations of bound and free hydroxyls, the stretching of carbonyl C=O bonds at 1 740 cm^{-1}, bending of free and bound hydroxyls at 1 620 and 1 380 cm^{-1}, respectively, stretching of C=C bonds of sp^2 hybridized carbons at 1 570 cm^{-1}, the asymmetric stretching of the epoxides C-O-C bonds at 1 240 cm^{-1}, the stretching of C-O and C-C bonds at 1 080 and 1 000 cm^{-1}, respectively, and bending vibrations of C-O-C at 850 cm^{-1} [41]. When GO is reduced, all bands related to hydroxyl groups are diminished while the intensity of C=C stretching band is expected to increase. Unfortunately, the IR vibrations of the individual components overlap to such extent that effective reduction of GO cannot be unequivocally deduced by IR.

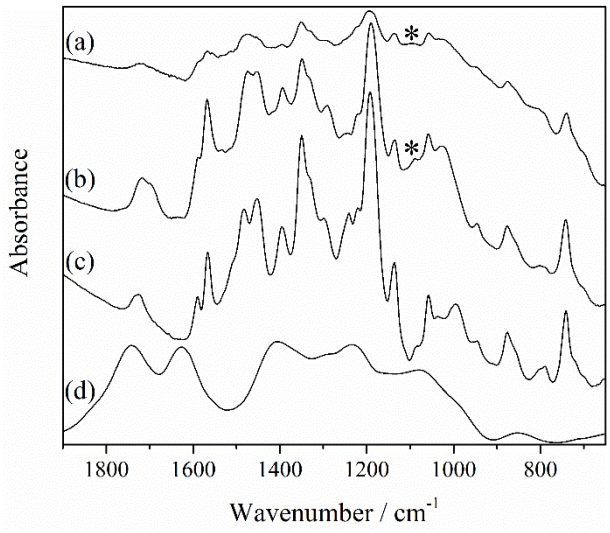

Fig. 7 IR spectra of (a) PAz/GO composite, (b) PAz/ErGO composite, (c) PAz and (d) GO. The peak related to GO in the composite materials' spectra is designated with an asterisk.

3.2.4 Raman spectroscopy

The Raman spectrum of PAz has been previously studied by several excitation wavelengths and the spectra have shown strong dependence of the laser wavelength which is related to different units in the structure being differently resonance enhanced depending on the excitation energy [40,41]. The *ex situ* Raman spectra of PAz, PAz/GO and PAz/ErGO composite films obtained using excitation wavelength of 785 nm are depicted in Fig. 8 and the Raman spectra of PAz and PAz/GO composite films obtained using excitation wavelength of 532 nm are depicted in Fig. S6. All Raman bands are listed in Table S2., and the UV-Vis spectra of PAz and PAz/GO films obtained on ITO coated quartz glass are presented in Fig. S7. The UV-Vis spectra of PAz and PAz/GO show an absorption

band at approximately 430 nm related to the π-π* transition of PAz [42]. The excitation wavelength of 532 nm is closer to the absorption maximum of PAz than GO and therefore this excitation wavelength should give information on the Raman lines originating from neutral parts of the polymer [40,41]. The Raman spectrum of PAz obtained using λ_{exc} = 532 nm gives rise to similar spectra obtained using 514 nm laser [41]. A doublet is observed at 1 564 and 1 531 cm^{-1} and the other bands lie at 1 393, 1 259, 1 220 and 1 041 cm^{-1}. The characteristic D and G bands of GO could not be well-distinguished from the Raman spectra obtained at 532 nm excitation wavelength although the peak at 1 394 cm^{-1} is broader than that observed in PAz Raman spectrum which could be attributed to the graphitic D band.

PAz Raman spectrum obtained with 785 nm laser (Fig. 8) exhibits bands at 1 546 cm^{-1} with shoulder at 1 495 cm^{-1} and at 1 385, 1 259, 1 205 and 1 044 cm^{-1}. Compared to the spectrum obtained at 532 nm excitation wavelength, the first bands lie at lower wavenumbers and, additionally, instead of a doublet a singlet is observed. This is in accordance with previous findings [41]. Tentative assignations have been made based on previous results with other aromatic polymers [43,44]. The most intense peak at 1 546 cm^{-1} is assigned to the stretching of C=C bonds while the shoulder at 1 495 cm^{-1} could be related to the stretching of C-C. Signals around 1 385 cm^{-1} have been previously attributed to the graphitic D band [40]. Combination of C-C stretching and C-H bending vibrations are assigned to 1 259 and 1 205 cm^{-1} [43]. GO and ErGO give rise to very well-known G and D bands at Raman shifts around 1 590 and 1 300 cm^{-1}, respectively, depicted in Fig. 8 with dashed lines. The D band is related to the defects in the sp^2 lattice and, therefore, the reduction of GO to ErGO should change the ratio of D to G band intensity and cause a shift of the bands to higher energies [45]. In the Raman spectra of PAz/GO composite obtained using λ_{exc} = 785 nm (Fig. 8b) clear signals originating from D and G modes of GO are visible at 1 571 and 1 314 cm^{-1}. In addition, a shoulder at 1 505 cm^{-1} is observed related to the polymer backbone as well as bands at 1 210 and 1 039 cm^{-1}. In the reduced composites spectrum, PAz related signals at 1 530, 1 380, 1 214 and 1 035 cm^{-1} are visible as well as a shoulder at 1 303 cm^{-1} which could be related to ErGO. Though the defect related D band would appear to be more intense in the PAz/GO than in the PAz/ErGO composite spectra, it is impossible to deduce the state of the reduction from Raman results due to the extensive overlapping of the two individual components' signals.

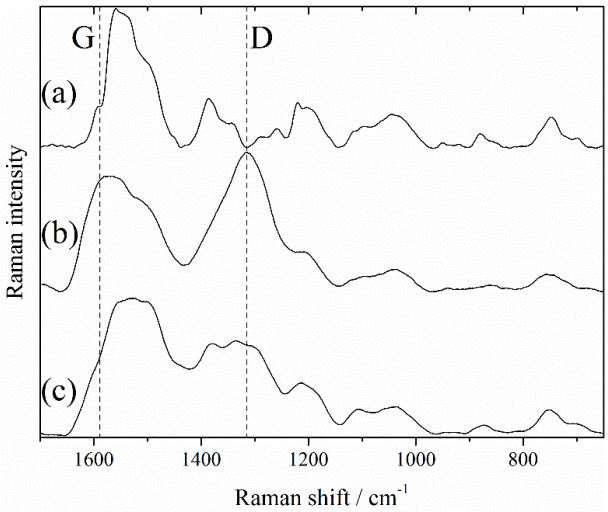

Fig 8. Raman spectra of (a) PAz, (b) PAz/GO composite and (c) PAz/ErGO composite films polymerized on gold coated Si wafers. The spectra was obtained using excitation wavelength λ_{exc} = 785 nm.

3.2.5 X-ray photoelectron spectroscopy

XPS was applied to verify both the incorporation of GO into PAz/GO composite film as well as efficient reduction of GO in PAz/ErGO composites. The C 1s XPS spectra of PAz, PAz/GO and PAz/ErGO films are presented in Fig. 9. During polymerization process, both GO and the IL are incorporated in the film, and additionally the complete removal of IL residue from the film is very difficult. These features are clearly observed in the XPS results. In all three films, the most intense de-convoluted peak centered at 284.7 eV is attributed to C-C and C=C bonds of both the polymer backbone as well as GO and ErGO [21]. Additionally, in all C 1s spectra peaks are found at 292.6, 290.8, 289.1, 287.8, 286.6 and 285.7 eV. Peaks at 290.8 and 292.6 eV are assigned to C-F bonds of perfluorinated species (CF_2 and CF_3, respectively), which originate from the doping anion [46,47]. From the XPS survey data (Fig. S8), it is evident that the samples are also composed of small amounts of nitrogen and sulfur which are attributed to ionic liquid residue (choline cation and TFSI anion, respectively) in the film. The C-S/C-N de-convoluted peak is found at 285.7 eV. The peak centered at 286.6 eV is attributed to C-O. In PAz, this is related to the hydroxyl group of choline cation residue. In the spectra of the GO composite, the relative amount of C-O increases slightly which is caused by the hydroxyl and epoxy groups on the plane and edges of GO sheets, and correspondingly in the spectra of ErGO composite the relative amount of C-O decreases (Table S3) to similar value observed in PAz which is attributed to the reduction of GO [21]. In addition, the atomic concentrations of oxygen are 15, 19 and 16 % for PAz, PAz/GO and PAz/ErGO, respectively, and a decrease and an increase in the C:O ratio (Table 1) is detected upon the addition

and reduction of GO, respectively. This verifies the incorporation and successful electroreduction of the composite. However, the differences in C:O ratio are not as profound as previously reported for ECP/GO composites which could be a result of partial reduction of GO already during electropolymerization [11]. Usually, the peaks centered at 287.8 and 289.1 eV are assigned to C=O and O-C=O, and in the case of the composites, the oxygen functional groups on GO and ErGO may contribute to these signals [21]. However, these species are not present in PAz or in the IL used, but the peaks are clearly existing in PAz C 1s spectrum. One explanation could be over-oxidation of the polymer, but there was no evidence of such occurrence in the other analysis results (IR). These peaks can also be attributed to covalent (289.1 eV) and 'semi-ionic' (287.8 eV) C-F bonds of the doping anion [47,48]. Both covalent and 'semi-ionic' types are distinguished in the F 1s spectra (Fig. S9).

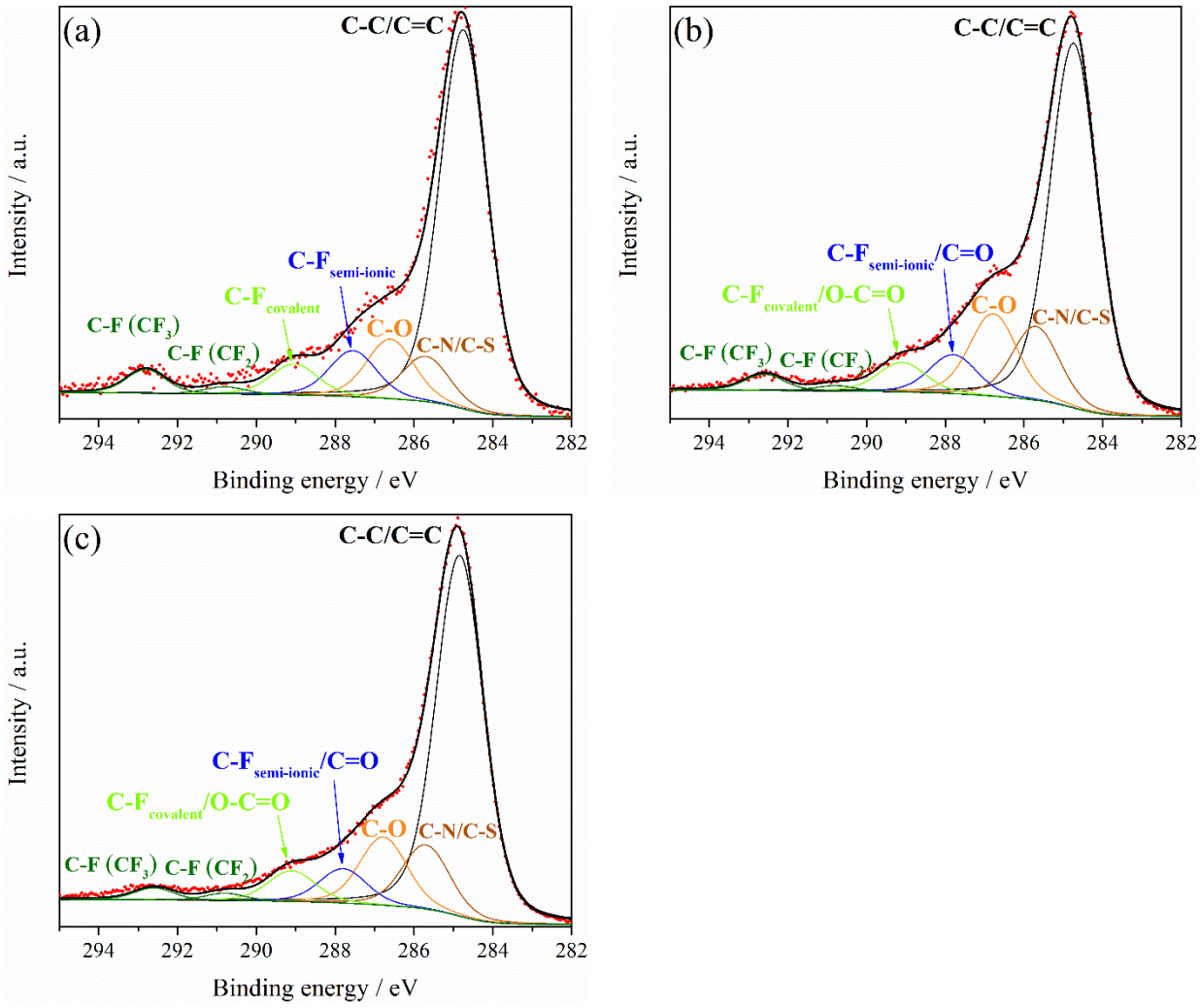

Fig. 9 C 1s XPS spectra of (a) PAz, (b) PAz/GO composite and (c) PAz/ErGO composite films.

Table 1. Atomic concentrations and C:O ratio calculated from the atomic concentrations.

	S (%)	C (%)	N (%)	O (%)	F (%)	C:O
PAz	2	70	4	15	9	4.6
PAz/GO	1	69	6	19	5	3.6
PAz/ErGO	1	78	1	16	4	4.8

4. Conclusions

We have successfully polymerized composites of polyazulene and reduced graphene oxide in a choline based ionic liquid by a facile electrochemical synthesis procedure. In conventional three-electrode configuration, the reduced composite materials showed capacitances of 94 ± 0.2 mF cm^{-2} ($PAz/GO_{0.1\ mg/mL}$), 130 ± 8 mF cm^{-2} ($PAz/GO_{1\ mg/mL}$) and 93 ± 11 mF cm^{-2} ($PAz/GO_{2\ mg/mL}$) at 20 mV s^{-1} scan rate while the capacitance of neat polymer under the same conditions was 55 ± 7 mF cm^{-2}. Highest capacitances were obtained using GO concentration of 1 mg mL^{-1} in [Choline][TFSI] though all composites exhibited higher capacitance than PAz alone and the differences between various GO concentration are small. All films exhibited good long term cycling stability but a tendency towards better cycling stability is reported for the composite material. By SEM we determined that the morphologies of the GO and ErGO composites varied significantly with large crumpled sheets of GO governing the structure of PAz/GO composite materials while a porous granule-like polymer matrix could be observed with evenly embedded ErGO sheets for the electrochemically reduced composite. The structural analysis by different spectroscopic techniques further verified the successful incorporation of GO into PAz as well as the reduction to ErGO. Since these composite materials possess a pseudo rectangular CV and good long term cycling ability, they are well suited as active components for supercapacitor application.

Acknowledgements

Funding from The Real Estate Foundation and University of Turku Graduate School (UTUGS) Doctoral Programme in Physical and Chemical Sciences are gratefully acknowledged for funding. Mauri Nauma is acknowledged for technical help with cell designs.

References

[1] L. Nyholm, G. Nyström, A. Mihranyan, M. Strømme, Toward Flexible Polymer and Paper-Based Energy Storage Devices, Adv. Mater. 23 (2011) 3751–3769. doi:10.1002/adma.201004134.

[2] E. Frackowiak, V. Khomenko, K. Jurewicz, K. Lota, F. Béguin, Supercapacitors based on conducting polymers/nanotubes composites, J. Power Sources. 153 (2006) 413–418.

doi:10.1016/j.jpowsour.2005.05.030.

[3] V. Mottaghitalab, G.M. Spinks, G.G. Wallace, The influence of carbon nanotubes on mechanical and electrical properties of polyaniline fibers, Synth. Met. 152 (2005) 77–80. doi:10.1016/j.synthmet.2005.07.154.

[4] A.K. Geim, K.S. Novoselov, The rise of graphene, Nat. Mater. 6 (2007) 183–191. doi:10.1038/nmat1849.

[5] M.D. Stoller, S. Park, Y. Zhu, J. An, R.S. Ruoff, Graphene-Based Ultracapacitors, Nano Lett. 8 (2008) 3498–3502. doi:10.1021/nl802558y.

[6] M. Hirata, T. Gotou, S. Horiuchi, M. Fujiwara, M. Ohba, Thin-film particles of graphite oxide 1:, Carbon 42 (2004) 2929–2937. doi:10.1016/j.carbon.2004.07.003.

[7] A. Burke, Ultracapacitor technologies and application in hybrid and electric vehicles, Int. J. Energy Res. 34 (2010) 133–151. doi:10.1002/er.1654.

[8] Y. Sun, G. Shi, Graphene/polymer composites for energy applications, J. Polym. Sci. Part B Polym. Phys. 51 (2013) 231–253. doi:10.1002/polb.23226.

[9] K. Zhang, L.L. Zhang, X.S. Zhao, J. Wu, Graphene/Polyaniline Nanofiber Composites as Supercapacitor Electrodes, Chem. Mater. 22 (2010) 1392–1401. doi:10.1021/cm902876u.

[10] J. Zhang, X.S. Zhao, Conducting Polymers Directly Coated on Reduced Graphene Oxide Sheets as High-Performance Supercapacitor Electrodes, J. Phys. Chem. C. 116 (2012) 5420–5426. doi:10.1021/jp211474e.

[11] B. Gadgil, P. Damlin, M. Heinonen, C. Kvarnström, A facile one step electrostatically driven electrocodeposition of polyviologen–reduced graphene oxide nanocomposite films for enhanced electrochromic performance, Carbon 89 (2015) 53–62. doi:10.1016/j.carbon.2015.03.020.

[12] P. Damlin, M. Suominen, M. Heinonen, C. Kvarnström, Non-covalent modification of graphene sheets in PEDOT composite materials by ionic liquids, Carbon 93 (2015) 533–543. doi:10.1016/j.carbon.2015.05.055.

[13] S. Lehtimäki, M. Suominen, P. Damlin, S. Tuukkanen, C. Kvarnström, D. Lupo, Preparation of Supercapacitors on Flexible Substrates with Electrodeposited PEDOT/Graphene Composites, ACS Appl. Mater. Interfaces. 7 (2015) 22137–22147. doi:10.1021/acsami.5b05937.

[14] J.M. Pringle, O. Ngamna, C. Lynam, G.G. Wallace, M. Forsyth, D.R. MacFarlane, Conducting Polymers with Fibrillar Morphology Synthesized in a Biphasic Ionic Liquid/Water System, Macromolecules. 40 (2007) 2702–2711. doi:10.1021/ma062483i.

[15] J.M. Pringle, O. Ngamna, J. Chen, G.G. Wallace, M. Forsyth, D.R. MacFarlane, Conducting

polymer nanoparticles synthesized in an ionic liquid by chemical polymerisation, Synth. Met. 156 (2006) 979–983. doi:10.1016/j.synthmet.2006.06.009.

[16] D. Wei, C. Kvarnström, T. Lindfors, A. Ivaska, Polyaniline nanotubules obtained in room-temperature ionic liquids, Electrochem. Commun. 8 (2006) 1563–1566. doi:10.1016/j.elecom.2006.07.024.

[17] A. Österholm, C. Kvarnström, A. Ivaska, Ionic liquids in electrosynthesis and characterization of a polyazulene-fullerene composite, Electrochim. Acta. 56 (2011) 1490–1497. doi:10.1016/j.electacta.2010.09.089.

[18] A. Österholm, T. Lindfors, J. Kauppila, P. Damlin, C. Kvarnström, Electrochemical incorporation of graphene oxide into conducting polymer films, Electrochim. Acta. 83 (2012) 463–470. doi:10.1016/j.electacta.2012.07.121.

[19] T. Lindfors, R.-M. Latonen, Improved charging/discharging behavior of electropolymerized nanostructured composite films of polyaniline and electrochemically reduced graphene oxide, Carbon 69 (2014) 122–131. doi:10.1016/j.carbon.2013.11.074.

[20] T. Lindfors, A. Österholm, J. Kauppila, R.E. Gyurcsányi, Enhanced electron transfer in composite films of reduced graphene oxide and poly(N-methylaniline), Carbon 63 (2013) 588–592. doi:10.1016/j.carbon.2013.07.022.

[21] T. Lindfors, A. Österholm, J. Kauppila, M. Pesonen, Electrochemical reduction of graphene oxide in electrically conducting poly(3,4-ethylenedioxythiophene) composite films, Electrochim. Acta. 110 (2013) 428–436. doi:10.1016/j.electacta.2013.03.070.

[22] G. Nöll, J. Daub, M. Lutz, K. Rurack, Synthesis, Spectroscopic Properties, and Electropolymerization of Azulene Dyads, J. Org. Chem. 76 (2011) 4859–4873. doi:10.1021/jo200080v.

[23] H. Xin, C. Ge, X. Yang, H. Gao, X. Yang, X. Gao, Biazulene diimides: a new building block for organic electronic materials, Chem. Sci. 7 (2016) 6701–6705. doi:10.1039/C6SC02504H.

[24] F. Wang, Y.H. Lai, N.M. Kocherginsky, Y.Y. Kosteski, The first fully characterized 1,3-polyazulene: High electrical conductivity resulting from cation radicals and polycations generated upon protonation, Org. Lett. 5 (2003) 995–998. doi:10.1021/ol0274615.

[25] R.-M. Latonen, B. Meana Esteban, C. Kvarnström, A. Ivaska, Electrochemical polymerization and characterization of a poly(azulene)-TiO2 nanoparticle composite film, J. Appl. Electrochem. 39 (2009) 653–661. doi:10.1007/s10800-008-9705-1.

[26] R.-M. Latonen, C. Kvarnström, A. Ivaska, Electrochemical preparation of oligo(azulene) on nanoporous TiO2 and characterization of the composite layer, J. Appl. Electrochem. 40 (2010) 1583–1591. doi:10.1007/s10800-010-0143-5.

[27] E. Grodzka, K. Winkler, B.M. Esteban, C. Kvarnstrom, Capacitance properties of electrochemically deposited polyazulene films, Electrochim. Acta. 55 (2010) 970–978. doi:10.1016/j.electacta.2009.09.054.

[28] R.-M. Latonen, A. Österholm, C. Kvarnström, A. Ivaska, Electrochemical and Spectroelectrochemical Study of Polyazulene/BBL-PEO Donor–Acceptor Composite Layers, J. Phys. Chem. C. 116 (2012) 23793–23802. doi:10.1021/jp308420s.

[29] M. Suominen, S. Lehtimäki, R. Yewale, P. Damlin, S. Tuukkanen, C. Kvarnström, Electropolymerized polyazulene as active material in flexible supercapacitors, J. Power Sources. 356 (2017) 181–190. doi:10.1016/j.jpowsour.2017.04.082.

[30] N. He, R.E. Gyurcsányi, T. Lindfors, Electropolymerized hydrophobic polyazulene as solid-contacts in potassium-selective electrodes, Analyst. 141 (2016) 2990–2997. doi:10.1039/C5AN02664D.

[31] R. Leones, J.M.S.S. Esperança, A. Pawlicka, V. de Zea Bermudez, M.M. Silva, Polymer electrolyte based on DNA and N,N,N-trimethyl-N-(2-hydroxyethyl)ammonium bis(trifluoromethylsulfonyl)imide, J. Electroanal. Chem. 748 (2015) 70–75. doi:10.1016/j.jelechem.2015.04.019.

[32] J.C. Dias, M.S. Martins, S. Ribeiro, M.M. Silva, J.M.S.S. Esperança, C. Ribeiro, G. Botelho, C.M. Costa, S. Lanceros-Mendez, Electromechanical actuators based on poly(vinylidene fluoride) with $[N_{1112(OH)}][NTf_2]$ and $[C_2mim]$ $[C_2SO_4]$, J. Mater. Sci. 51 (2016) 9490–9503. doi:10.1007/s10853-016-0193-0.

[33] A. Österholm, B.M. Esteban, C. Kvarnström, A. Ivaska, Spectroelectrochemical study of the redox reactions of polyazulene on aluminum substrates, J. Electroanal. Chem. 613 (2008) 160–170. doi:10.1016/j.jelechem.2007.10.022.

[34] A.J.L. Costa, M.R.C. Soromenho, K. Shimizu, I.M. Marrucho, J.M.S.S. Esperanca, J.N.C. Lopes, L.P.N. Rebelo, Density, thermal expansion and viscosity of cholinium-derived ionic liquids, ChemPhysChem. 13 (2012) 1902–1909. doi:10.1002/cphc.201100852.

[35] T. Yong, L. Zhang, J. Wang, Y. Mai, X. Yan, X. Zhao, Novel choline-based ionic liquids as safe electrolytes for high-voltage lithium-ion batteries, J. Power Sources. 328 (2016) 397–404. doi:10.1016/j.jpowsour.2016.08.044.

[36] L. Tanzi, P. Benassi, M. Nardone, F. Ramondo, Vibrations of Bioionic Liquids by Ab Initio Molecular Dynamics and Vibrational Spectroscopy, J. Phys. Chem. A. 118 (2014) 12229–12240. doi:10.1021/jp5079949.

[37] V.H. Paschoal, L.F.O. Faria, M.C.C. Ribeiro, Vibrational Spectroscopy of Ionic Liquids, Chem. Rev. 117 (2017) 7053–7112. doi:10.1021/acs.chemrev.6b00461.

559 [38] M. Acik, G. Lee, C. Mattevi, M. Chhowalla, K. Cho, Y.J. Chabal, Unusual infrared-
560 absorption mechanism in thermally reduced graphene oxide, Nat. Mater. 9 (2010) 840–845.
561 doi:10.1038/nmat2858.
562 [39] J. Kauppila, P. Kunnas, P. Damlin, A. Viinikanoja, C. Kvarnström, Electrochemical
563 reduction of graphene oxide films in aqueous and organic solutions, Electrochim. Acta. 89
564 (2013) 84–89. doi:10.1016/j.electacta.2012.10.153.
565 [40] B. Meana-Esteban, C. Lete, C. Kvarnström, A. Ivaska, Raman and in situ FTIR-ATR
566 characterization of polyazulene films and its derivate, J. Phys. Chem. B. 110 (2006) 23343–
567 23350. doi:10.1021/jp0631811.
568 [41] A. Österholm, B. Meana-Esteban, C. Kvarnström, A. Ivaska, In situ Resonance Raman
569 Spectroscopy of Polyazulene on Aluminum, J. Phys. Chem. B. 112 (2008) 6331–6337.
570 doi:10.1021/jp0762828.
571 [42] G. Nöll, C. Lambert, M. Lynch, M. Porsch, J. Daub, Electronic Structure and Properties of
572 Poly- and Oligoazulenes, J. Phys. Chem. C. 112 (2008) 2156–2164. doi:10.1021/jp074376b.
573 [43] P. Damlin, C. Kvarnström, A. Petr, P. Ek, L. Dunsch, A. Ivaska, In situ resonant Raman and
574 ESR spectroelectrochemical study of electrochemically synthesized poly(p-
575 phenylenevinylene), J. Solid State Electrochem. 6 (2002) 291–301.
576 doi:10.1007/s100080100240.
577 [44] H. Bai, X. Wu, G. Shi, Synthesis and characterization of poly(1,5-naphthylene vinylene) and
578 its copolymers with poly(2-methoxy-5-(2′-ethylhexyloxy)-p-phenylene vinylene), Polymer
579 47 (2006) 1533–1537. doi:10.1016/j.polymer.2006.01.004.
580 [45] G.K. Ramesha, S. Sampath, Electrochemical Reduction of Oriented Graphene Oxide Films:
581 An in Situ Raman Spectroelectrochemical Study, J. Phys. Chem. C. 113 (2009) 7985–7989.
582 doi:10.1021/jp811377n.
583 [46] E.P. Dillon, C.A. Crouse, A.R. Barron, Synthesis, Characterization, and Carbon Dioxide
584 Adsorption of Covalently Attached Polyethyleneimine-Functionalized Single-Wall Carbon
585 Nanotubes, ACS Nano. 2 (2008) 156–164.
586 [47] J.M. Pringle, O. Winther-Jensen (née Ngamna), C. Lynam, G.G. Wallace, M. Forsyth, D.R.
587 MacFarlane, One-Step Synthesis of Conducting Polymer–Noble Metal Nanoparticle
588 Composites using an Ionic Liquid, Adv. Funct. Mater. 18 (2008) 2031–2040.
589 doi:10.1002/adfm.200701147.
590 [48] A. Tressaud, F. Moguet, S. Flandrois, M. Chambon, C. Guimon, G. Nanse, E. Papirer, V.
591 Gupta, O.P. Bahl, On the nature of C-F bonds in various fluorinated carbon materials: XPS
592 and TEM investigations, J. Phys. Chem. Solids. 75 (1996) 745–751.

593